Clean Graphene Surfaces



A Force-Engineered Lint Roller for Superclean Graphene

Luzhao Sun, Li Lin, Zihao Wang, Dingran Rui, Zhiwei Yu, Jincan Zhang, Yanglizhi Li, Xiaoting Liu, Kaicheng Jia, Kexin Wang, Liming Zheng, Bing Deng, Tianbao Ma, Ning Kang, Hongqi Xu, Konstantin S. Novoselov, Hailin Peng,* and Zhongfan Liu*

Contamination is a major concern in surface and interface technologies. Given that graphene is a 2D monolayer material with an extremely large surface area, surface contamination may seriously degrade its intrinsic properties and strongly hinder its applicability in surface and interfacial regions. However, large-scale and facile treatment methods for producing clean graphene films that preserve its excellent properties have not yet been achieved. Herein, an efficient postgrowth treatment method for selectively removing surface contamination to achieve a large-area superclean graphene surface is reported. The as-obtained superclean graphene, with surface cleanness exceeding 99%, can be transferred to dielectric substrates with significantly reduced polymer residues, yielding ultrahigh carrier mobility of 500 000 cm² V $^{-1}$ s $^{-1}$ and low contact resistance of 118 Ω μ m. The successful removal of contamination is enabled by the strong adhesive force of the activated-carbon-based lint roller on graphene contaminants.

The progress of modern semiconductor industry relies on effective surface-cleaning techniques.^[1] The increasing applications of graphene and other 2D materials depend highly on the availability of superclean surfaces, because surface cleanness significantly affects the properties and performances of such materials, especially considering their 2D natures.^[2–7] Although chemical vapor deposition (CVD)-derived graphene film on metal foil shows promising properties,^[8,9] it still faces the serious issue of surface contamination, which strongly degrades the graphene properties.^[3,6,7]

Surface contamination of CVD-derived graphene films has three main origins: intrinsic contamination that occurs during the CVD growth process (Note S1, Supporting Information), polymer residues introduced by transfer processes from the growth substrate to the target substrate,^[10] and airborne contaminants.^[5] Many attempts have been made to remove surface contaminants from graphene via annealing,^[10–12] plasma treatment,^[13,14] and mechanical cleaning,[15,16] which have been proven to be effective. However, only emphasizing the elimination of transfer-related contamination, these postgrowth routines cannot thoroughly solve the issue of surface contamination. Obtaining superclean graphene film on a large scale is thus a major hurdle in graphene research (Table S1, Supporting Information). In this paper, we obtain

a meter-sized superclean graphene film, relying on the direct effective cleaning of graphene on Cu foil to eliminate the intrinsic surface contamination, i.e., amorphous carbon, [17] immediately following CVD growth. In this case, amorphous carbon is successfully removed using an activated carbon-coated lint roller that has a strong adhesive interaction with amorphous carbon. The successful removal of amorphous carbon would contribute to reducing the polymer residues on graphene during the transferring process, as well as enhancing the optical and electrical properties.

L. Z. Sun, Dr. L. Lin, Dr. J. C. Zhang, Y. L. Z. Li, X. T. Liu, K. C. Jia, K. X. Wang, L. M. Zheng, Dr. B. Deng, Prof. H. L. Peng, Prof. Z. F. Liu Center for Nanochemistry
Beijing Science and Engineering Center for Nanocarbons
Beijing National Laboratory for Molecular Sciences
College of Chemistry and Molecular Engineering
Peking University
Beijing 100871, P. R. China
E-mail: hlpeng@pku.edu.cn; zfliu@pku.edu.cn
L. Z. Sun, Dr. J. C. Zhang, Y. L. Z. Li, X. T. Liu
Academy for Advanced Interdisciplinary Studies
Peking University
Beijing 100871, P. R. China

The ORCID identification number(s) for the author(s) of this article can be found under https://doi.org/10.1002/adma.201902978.

DOI: 10.1002/adma.201902978

School of Physics and Astronomy University of Manchester Manchester M13 9PL, UK D. R. Rui, Prof. N. Kang, Prof. H. Q. Xu Beijing Key Laboratory of Quantum Devices Key Laboratory for the Physics and Chemistry of Nanodevices, and Department of Electronics **Peking University** Beijing 100871, P. R. China Z. W. Yu. Prof. T. B. Ma State Key Laboratory of Tribology Tsinghua University Beijing 100084, P. R. China Prof. H. L. Peng, Prof. Z. F. Liu Beijing Graphene Institute Beijing 100095, P. R. China

Dr. L. Lin, Z. H. Wang, Prof. K. S. Novoselov

15214905, 2019, 43, Downloaded from https://onlinelibtrary.wiley.com/doi/10.1002/adma.20902978 by Sochow University. Wiley Online Library on [15/1/1/2024]. See the Terms and Conditions (https://onlinelibrary.wiley.com/terms-and-conditions) on Wiley Online Library for rules of use; OA archies are governed by the applicable Creative Commons License

www.advancedsciencenews.com

www.advmat.de

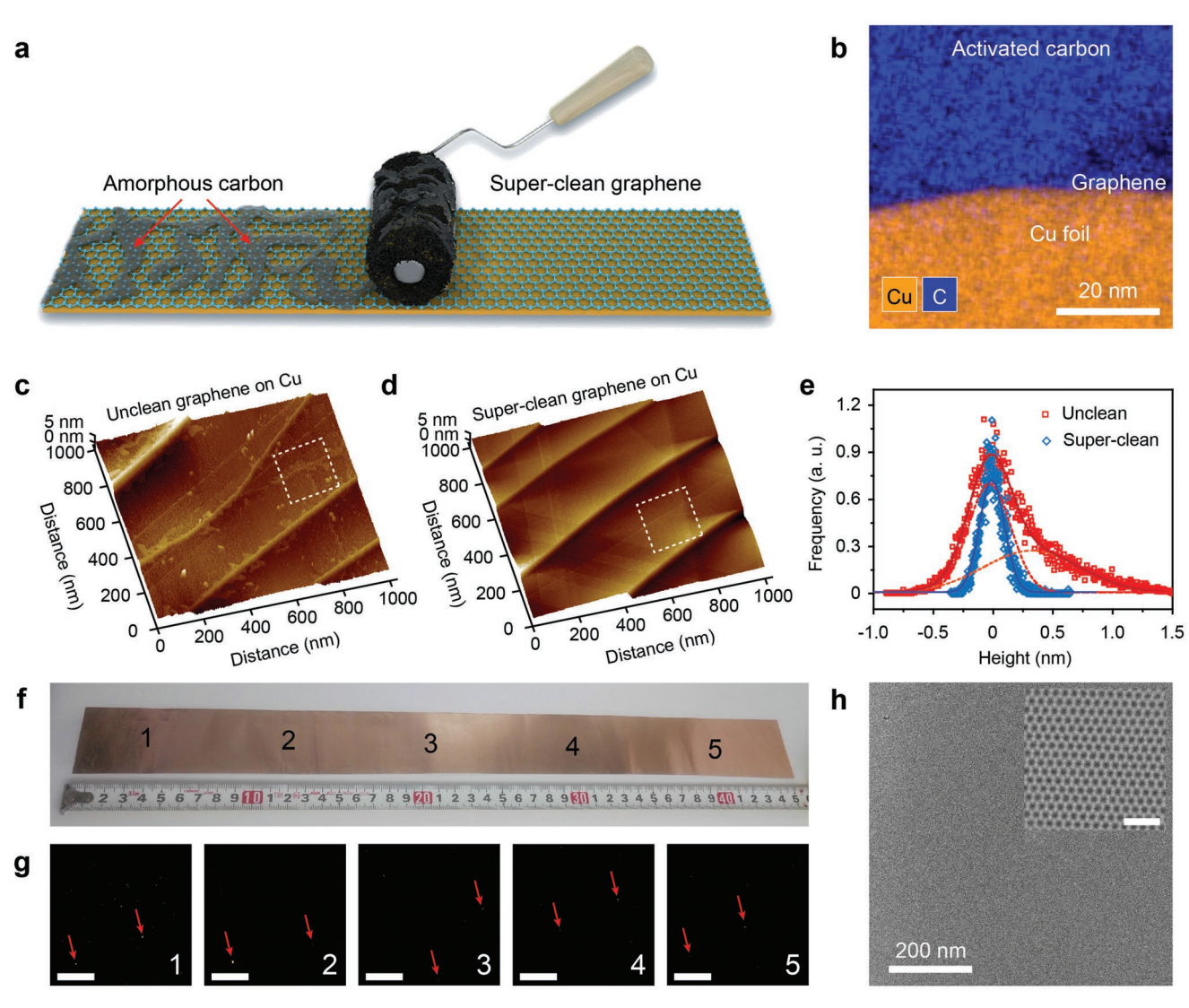


Figure 1. Superclean graphene treated by the activated carbon-coated lint roller. a) Schematic of the activated carbon-coated lint roller for cleaning the graphene surface. b) Cross-sectional EDS map of contact area between activated carbon and graphene. AFM images of c) unclean and d) superclean graphene on Cu foil. e) Histogram of the height distribution for unclean graphene and superclean graphene corresponding to the dashed box in (c) and (d), respectively. f,g) Large-area visualization of as-obtained superclean graphene through the selective deposition of TiO₂ particles (white dots in g); scale bar: 50 μm. h) HR-TEM image showing the atomically clean surface. Inset: lattice image of superclean graphene with atomic resolution; scale bar: 2 nm.

During high-temperature CVD growth, graphene surfaces are contaminated with defective amorphous carbon with a thickness of a few nanometers (Figure S1, Supporting Information). Fortunately, the absence of relatively strong interactions between the amorphous carbon and graphene surface promise a possibility of detaching them for obtaining a clean graphene surface, as evident in the movement of amorphous carbon on a graphene surface as driven by an electron-beam (Figure S2, Supporting Information).

The typical lint roller, commonly used to remove dust from clothes in daily life, is composed of one-sided adhesive paper that interacts strongly with targeted contaminants. Inspired by this, an activated carbon-coated lint roller is fabricated to treat the graphene/Cu foil and obtain a clean graphene surface, relying on the strong interaction between the activated carbon

and amorphous carbon present on the graphene. In detail, activated carbon powder was coated on micrometer-sized pores of commercially available Cu foam to achieve a high mass loading of activated carbon; a binder was used to form a strong connection between Cu foam and activated carbon. The cleaning process of the as-received large area of graphene on Cu foil was conducted by slowly rolling the foil directly under the activated carbon-coated lint roller at a temperature of no more than 170 °C (Figure 1a and Figure S3, Supporting Information). Relying on the softness of annealed Cu foil, close contact between activated carbon and contaminants on graphene is permitted, which is confirmed by analysis using cross-sectional transmission electron microscopy (TEM) and energy dispersive spectrum (EDS) mapping (Figure 1b and Figure S4, Supporting Information).



www.advancedsciencenews.com



www.advmat.de

The removal of amorphous carbon contaminants from graphene after the lint rolling process is revealed by atomic force microscopy (AFM). As shown in Figure 1c, a typical AFM image of common CVD graphene samples before the cleaning process indicates that amorphous carbon is universally distributed over the entire graphene surface. After the lint-rolling post-treatment, much cleaner graphene with reduced surface contamination is observed (Figure 1d), as confirmed by the much narrower height distribution (Figure 1e) and improved surface flatness (Figure S5, Supporting Information) on the Cu terrace.

The efficient force-engineered lint rolling post-treatment allows the fabrication of a large-area superclean graphene surface. As shown in Figure 1f, a meter-scale superclean graphene sample is obtained, and the cleanness is evaluated through the visualization of surface contaminants using the TiO2 deposition method (Note S2 and Figure S6, Supporting Information).[18-20] As shown in Figure 1g, almost no TiO2 particles is on the dark-field optical microscopy images, which indicate the superclean nature of the as-obtained graphene sample. After transferring the as-received graphene onto the TEM grid, the high degree of surface cleanness of graphene film (reaching 99%) is further confirmed using high-resolution TEM (HR-TEM; Figure 1h and Figure S7, Supporting Information). Processing temperature and rolling speed are two important parameters for optimizing effectiveness of the post-treatment (Figure S8a, Supporting Information), where a higher temperature (no more than 170 °C) and slower rolling speed would be preferred. The recoverability test shows that the effectiveness of the activated carbon-coated lint roller could be maintained at least 40 rounds (Figure S8b, Supporting Information).

The availability of superclean graphene on Cu would enable the suppression of contamination by polymer residues in the following transfer step for further applications. Normally, a transfer process of graphene from the growth substrate to a dielectric substrate is required for further device fabrication and integration.[21-23] In such processes, a polymer medium such as poly(methyl methacrylate) (PMMA) is usually used to support the graphene film. This unfortunately results in significant PMMA residues on the as-transferred graphene surface, [6,24] as evident in the AFM image of unclean graphene transferred onto atomically flat mica, where the polymer residue is clearly visible (Figure 2a). The height distribution (Figure 2b) is fitted with three Gaussian peaks, which can be assigned to graphene, amorphous carbon, and PMMA residues. In contrast, almost no PMMA residues or amorphous carbon is found on the surface of the as-obtained superclean graphene after the transfer (Figure 2c), as indicated by the similar height distribution of the as-transferred superclean graphene with that of mica (Figure 2d). Clearly, the removal of amorphous carbon before transfer ensures the reduction of transfer-related polymer residues. Figure 2e displays a photograph of a superclean graphene film transferred onto a large-area (around 4 in. size) mica substrate. The corresponding AFM images and the statistical data reveal a cleanness of ≈99% after the transfer (Figure 2f and Figure S9, Supporting Information). Furthermore, the PMMA residues on common as-transferred graphene samples can also be removed efficiently by the activated carbon-coated lint roller (Figure S10, Supporting Information), demonstrating the universality of our method. To characterize the quality of the asobtained graphene, Raman characterization was conducted by randomly sampling the transferred graphene on SiO_2 substrate. In our results, almost no defect-related D peaks are observed and the 2D/G ratio is larger than 2 (Figure S11, Supporting Information), which confirms the high quality and monolayer nature.^[25]

To evaluate the electronic properties of as-obtained superclean graphene, contact resistance and carrier mobility, which are two parameters dominating the electrical performances of graphene devices in high-speed electronics, have been measured.^[26] A graphene transistor array (inset of Figure 3a) is fabricated for measuring the contact resistance. By using the transfer length method (TLM),^[27] we can extract the contact resistance at different gate bias voltages (V_G - V_{Dirac}, $V_{\rm Dirac} = 15$ V) at room temperature (Figure 3b and Figure S12, Supporting Information), where the minimum contact resistance between clean graphene and metal (Pd/Au) reaches 117.6 \pm 32.5 Ω µm at $V_G = V_{Dirac} - 37$ V, which is comparable with that of exfoliated graphene. [27] The field-effect mobility of the as-received superclean graphene on a SiO₂/Si substrate is approximately 17 100 cm² V⁻¹ s⁻¹ at 1.9 K, which indicates the contribution of the low contamination level to the improved electrical qualities (Figure S13, Supporting Information). [28,29] To further confirm the intrinsic mobility of superclean graphene, hexagonal boron nitride (hBN)-encapsulated graphene Hall bar devices with 1D edge contact (inset of Figure 3c) were fabricated using hot "pick-up" technique (see Experimental Section and Note S3 in the Supporting Information). [30,31] By plotting the four-terminal resistance as a function of the gate voltage (V_G), the extracted field-effect mobility is found to exceed 400 000 cm² V⁻¹ s⁻¹ at 1.7 K (Figure 3c), while the corresponding Hall mobility reaches 500 000 cm² V⁻¹ s⁻¹ (Figure 3d). By performing magnetotransport measurements on the hBN-encapsulated graphene Hall bar device, the Landau fan and broken Landau level (LL) degeneracy can be well resolved (Figure 3e), indicating the ultrahigh quality of the as-received superclean graphene.

The reduced contamination also contributes to the reduced sheet resistance and improved optical transmittance, which are important parameters in the application of graphene as a transparent conductive film. The as-obtained superclean graphene film exhibits a lower sheet resistance (618.0 \pm 19.6 Ω \Box ⁻¹) than that of unclean graphene film (879.8.0 \pm 173.7 Ω \Box ⁻¹) (Figure S14a, Supporting Information), which is probably ascribable to the increase in carrier mobility and improved contact. As for the optical transmittance, the superclean graphene transferred on quartz glass exhibits an average transmittance of 97.4% at a wavelength of 550 nm, which is very close to the ideal value of monolayer graphene (Figure S14b, Supporting Information).[32] By stacking three layers of graphene on a polyethylene terephthalate (PET) substrate via layer-by-layer transfer, the difference in transmittance between unclean and superclean graphene is observable by the naked eye (Figure S14c, Supporting Information).

The interfacial force model was proposed to investigate the cleaning mechanism of the activated carbon-coated lint roller, where two interfaces in lint-roll structure should be taken into consideration: 1) interface between activated carbon and

(https://onlinelibrary.wiley.com/terms-and-conditions) on Wiley Online Library for rules of use; OA articles are governed by the applicable Creative Commons License

www.advancedsciencenews.com

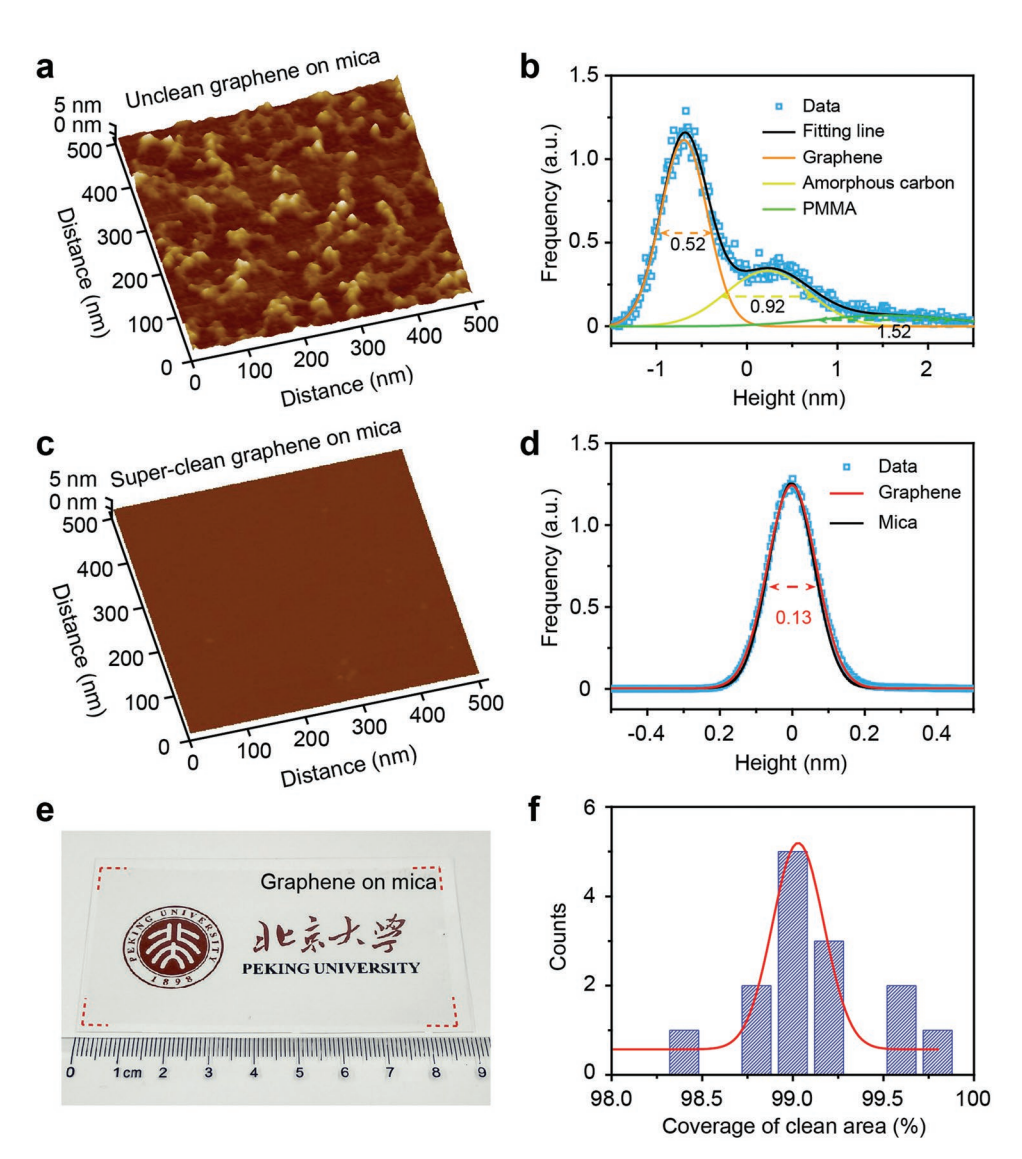


Figure 2. Suppression of polymer residue after graphene transfer. AFM image of a) unclean graphene on mica substrate and b) corresponding height distribution. AFM image of c) as-obtained superclean graphene on mica substrate and d) corresponding height distribution. e) An as-obtained largearea superclean graphene film transferred onto an around 4 in.-sized mica substrate. f) Cleanness histogram for the transferred superclean graphene.

amorphous carbon; 2) interface between amorphous carbon and graphene (Figure 4a). Activated carbon has a porous structure and many functional groups (Note S4 and Figure S15, Supporting Information), enabling stronger interaction with the amorphous carbon than that between the amorphous carbon and the graphene.^[33] The stronger interaction ensures successful detachment of the amorphous carbon from the graphene basal plane. To further confirm this, the adhesion forces between amorphous carbon and activated carbon (F– $C_{amorphous}$ – $C_{activated}$), and those between amorphous carbon and graphene (F-C_{amorphous}-Gr) were measured, respectively. An amorphous carbon-coated microsphere probe was fabricated and glued onto an AFM cantilever, which is used to measure the typical adhesive forces (Figure S16, Supporting Information). When amorphous carbon-coated microsphere probe gradually approaches toward the superclean graphene or the activated carbon, the adhesive forces between amorphous carbon/graphene(F– $C_{amorphous}$ –Gr) and those between amorphous carbon/activated carbon (F– $C_{amorphous}$ – $C_{activated}$) could be read out from the force-displacement curves (Figure 4b). F– $C_{amorphous}$ –Gr with an average value of 93.1 \pm 10.9 nN is clearly smaller than F– $C_{amorphous}$ – $C_{activated}$ (373.2 \pm 158.0 nN), confirming the capability of activated carbon to remove amorphous carbon from graphene surface. The adhesive energies (at contact per unit area) could be also evaluated via the Johnson–Kendall–Roberts theory, [34] using

$$W = \frac{2F_{\rm ad}}{3\pi R} \tag{1}$$

where F_{ad} is the adhesion force and R is the radius of the spherical tip. We find that the adhesive energy between amorphous carbon and activated carbon is $W = 15.8 \pm 6.7$ mJ m⁻², while the adhesive energy between amorphous carbon and

15214095, 2019, 43, Downloaded from https://onlinelibrary.wiley.com/doi/10.1002/adma.201092978 by Sochow University, Wiley Online Library on [1511/1024]. See the Terms and Conditions (https://onlinelibrary.wiley.com/errms-and-conditions) on Wiley Online Library for rules of use; OA articles are governed by the applicable Creative Commons Licensed

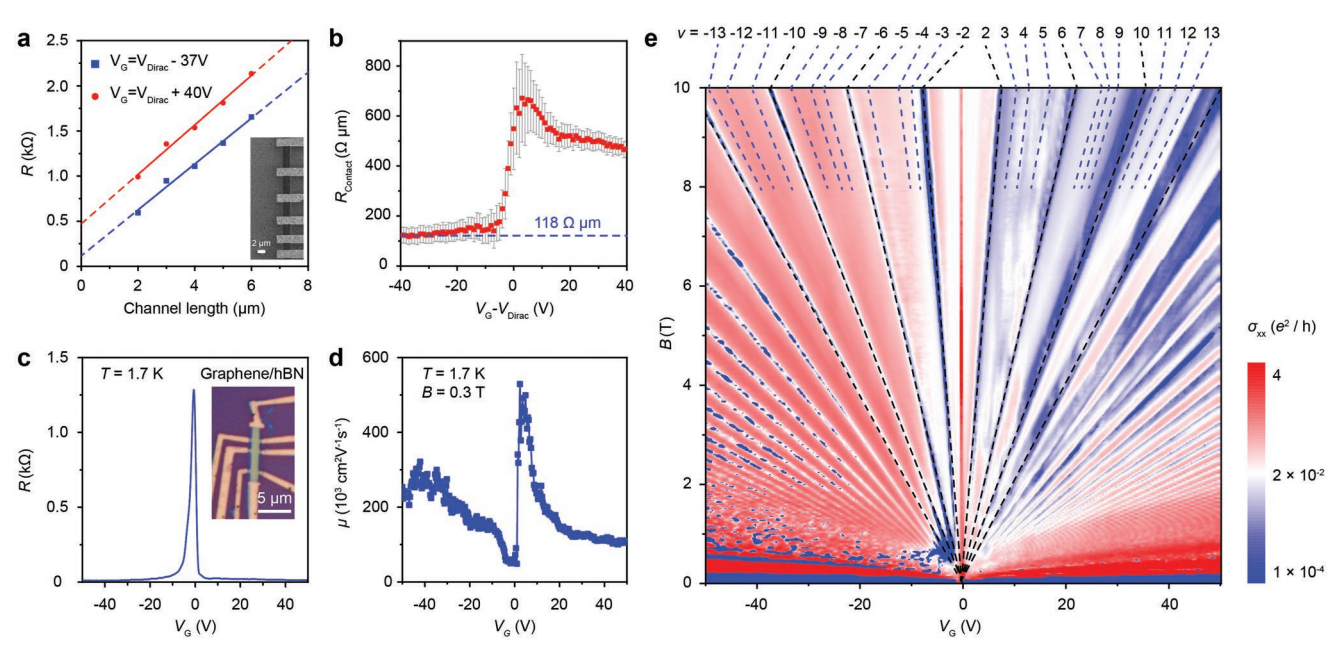


Figure 3. Superior electronic properties of as-obtained superclean graphene. a) Source drain resistance as functions of channel length at gate bias of $V_G = V_{Dirac} - 37 \text{ V}$ (green) and $V_G = V_{Dirac} + 40 \text{ V}$ (red). Contact resistance can be calculated according to the vertical intercept of linear fitting curve. Inset: SEM image of the TLM-measured graphene transistor array, where the channel lengths vary from 2 to 6 μm; scale bar: 2 μm. b) The contact resistance as a function of gate bias. c) Resistivity of superclean graphene encapsulated by hBN as a function of gate voltage (V_G) at T = 1.7 K. Inset: optical microscopy image of Hall bar device of encapsulated graphene with 1D contact. d) The Hall mobility as a function of back gate voltage (V_G), where, the carrier mobility near the Dirac point can exceed 500 000 cm² V⁻¹ s⁻¹. e) Longitudinal conductivity (σ_{α}) as a function of magnetic field B and V_G for the device in (c). The dash black lines clearly show LLs at filling factors $v = \pm 2, \pm 6, \pm 10...$, and some new emerging filling factors, due to the degeneracy lifting of LLs, are also indicated by the dash blue lines at $v = \pm 3, \pm 4, \pm 5$.

graphene is $W = 4.0 \pm 0.5$ mJ m⁻². These values are far less than the binding energy between graphene and its substrates, [35-37] which guarantees the intactness of the graphene films on substrate without detachment during the postgrowth treatment.

In summary, we developed and demonstrated an activated carbon-coated lint roller with a strong adhesive force to successfully remove surface contaminants from graphene surfaces. The as-treated graphene surface exhibited a high cleanness of 99% with a low degree of polymer residue after transfer onto a functional substrate. The superclean signature of the graphene film ensures considerably enhanced electrical and optical properties, providing a new material platform for various applications of graphene such as radio-frequency transistors. In the electrocatalytic field, high-quality superclean graphene might exhibit wider electrochemical potential window and better electrochemical stability compared to other carbon-based electrodes (such as glassy carbon electrodes), and therefore may serve as inert electrodes or electrocatalyst carriers. As for the application of graphene in lithium-ion batteries, superclean graphene could be used to study the lithium storage mechanism of intrinsic singlelayer graphene without the influence of the contaminants.

Experimental Section

Graphene-Film Growth: Graphene films were grown on Cu foil using a low-pressure CVD system, as reported previously. Typically, 25 µm thick Cu foil (99.8% purity, Alfa-Aesar #46365) was placed in a quartz tube

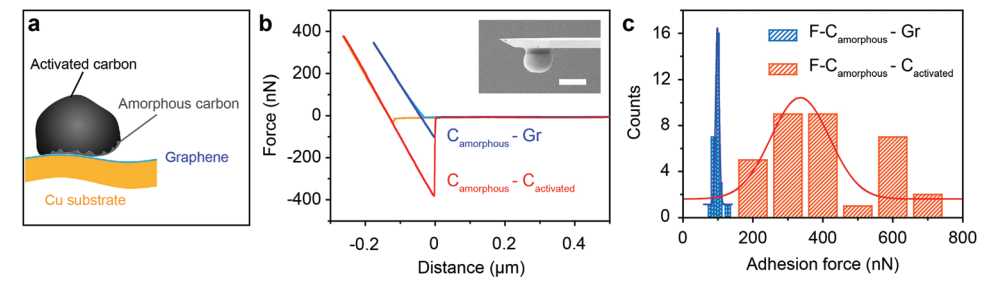


Figure 4. Force-engineered mechanism for cleaning graphene surface. a) Interfacial force model depicting activated carbon and unclean graphene on Cu foil. b) Typical measured adhesive forces of F-C_{amorphous}-C_{activated} (red curve) and F-C_{amorphous}-Gr (blue curve). Inset: SEM image of the as-fabricated AFM tip equipped by amorphous-carbon-coated microsphere probe; scale bar: 10 μm. c) Histograms of adhesion forces of Camorphous-Cactivated and Camorphous-Graphene measured using the same amorphous carbon-coated microsphere probe.

www.advancedsciencenews.com



www.advmat.de

furnace and heated to $1020\,^{\circ}\text{C}$ under a 500 sccm flow of Ar. The sample was then annealed for 30 min under a 500 sccm flow of H₂. Graphene was then grown for 20 min under a 100 sccm flow of H₂ and 1 sccm-flow of CH $_{\star}$.

Graphene-Film Cleaning Using the Activated Carbon-Coated Lint Roller: An activated carbon-coated lint-roller was fabricated by binding activated carbon powder to porous Cu foam with poly(vinylidene fluoride; PVDF, 1000 K). The mass ratio of activated carbon to PVDF was 6:1, and the binder solvent was N-methylpyrrolidone. Normal graphene on Cu foil was placed in a vacuum system and rolled by the as-fabricated activated-carbon lint roller at a temperature of no more than 170 °C. The graphene surfaces were usually cleaned four times by this procedure.

Graphene Transfer. The graphene was transferred onto a TEM grid using a nonpolymer-assisted method, as reported previously. The graphene film was transferred onto mica and SiO $_2$ with the assistance of PMMA. The graphene/Cu was spin-coated with PMMA at 2000 rpm and then baked at 170 °C for 5 min. After etching away the Cu foil with 1 $_{\mbox{\scriptsize M}}$ Na $_2\mbox{\scriptsize S}_2\mbox{\scriptsize O}_8$ solution and washing with deionised water, the PMMA/ graphene was subsequently placed onto target substrates and the PMMA was dissolved using acetone. A "dry" transfer method was used to fabricate hBN-encapsulated graphene devices, including the native oxidation of Cu, "pick-up" graphene by hBN and drop down steps (Note S3, Supporting Information). $^{[30,31]}$ Large-scale graphene films were transferred onto PET substrates with the assistance of thermal release tape.

Adhesion-Force Measurements: Adhesion force was measured in air on an MFP-3D atomic-force microscope (Asylum Research) fitted with a graphene-coated microsphere probe. Amorphous carbon was first coated on copper microspheres by growing dirty graphene. In order to fabricate the graphene-coated microsphere probe, the amorphous carbon-coated microsphere was then glued to an AFM cantilever (Nanosensor TL-FM), as previously reported. [39] The normal force constant ($k = 2.82 \text{ N m}^{-1}$) was calibrated using the thermal-noise method. [40]

Preparation of Cross-Sectional Specimens for TEM: A dual-beam TEM instrument (FEI Strata DB 235), which combines a focused-ion beam (FIB) and an scanning electron microscopy (SEM) column, was used to fabricate cross-sectional specimens of activated carbon/graphene/Cu foil. For initial surface protection during FIB scanning, the activated carbon/graphene/Cu sample was coated with a 30 nm thick Cr layer by thermal evaporation. A 1 μm Pt layer was then deposited at the selected region of the Cr/activated carbon/graphene/Cu structure as a protection layer as the sample was finally milled at thicknesses below 30 nm.

SEM and TEM Measurements: SEM images were acquired on a scanning electron microscope (Hitachi S-4800, accelerator voltage: 1–10 kV). The cross-sectional analysis of contact between activated carbon and amorphous carbon on graphene were conducted using aberration-corrected TEM (FEI Titan Cubed Themis G2 300) under 300 kV. The bright-field and high-angle annular dark-field images of graphene were acquired in the same aberration-corrected TEM under 80 kV.

Device Fabrication and Transport Measurements: To evaluate the electrical properties of our graphene sample, Hall bar devices and TLM devices were fabricated on the graphene crystal transferred onto 300 nm thick silicon oxide with alignments marks. The flatness of each sample was verified by AFM. Electron-beam lithography (Raith 150 2nd) and reactive ion etching with O2 (Trion Technology Minilock III) were employed to pattern graphene into a Hall bar geometry. After a PMMA mask (PMMA 950K A4 @ 4000 rpm) was patterned by EBL, Pd/Au (5/90 nm) electrodes were deposited by electron-beam evaporation (Kurte J. Lesker AXXIS). Electrical transport at room temperature was determined using a vacuum-probe station (Lake Shore TTP-4) with a Keithley semiconductor characterization system (Model 4200-SCS). Electrical and magnetotransport data at low temperatures were acquired using a physical property measurement system (PPMS, Quantum Design DynaCool). Device resistance was measured using a lock-in amplifier (Stanford Research 830) with an ac driving current of 50-100 nA.

Note that the sizes of characterized region by TEM, AFM, and dark-field optical microscopy methods were 1 μm^2 , 1 μm^2 , and 0.04 mm²,

respectively. To obtain more reliable results of cleanness, every around 8 cm in the entire sample, by transferring these regions to be sampled onto TEM grids with 3 mm diameter based on the TEM method, or by exposing the regions to be sampled under ${\rm TiCl_4}$ vapor based on the ${\rm TiO_2}$ visualizaiton method, was sampled. Then cleanness of graphene on TEM grid would be evaluated directly by TEM image, while the cleanness of graphene exposed to the ${\rm TiO_2}$ particles would be characterized by dark-field optical microscopy, where unclean region would be covered by ${\rm TiO_2}$ particles and become brighter than clean region.

Supporting Information

Supporting Information is available from the Wiley Online Library or from the author.

Acknowledgements

L.Z.S., L.L., Z.H.W., and D.R.R. contributed equally to this work. The authors thank Prof. Mark H. Rümmeli and Liang Zhao in Soochow University for the help on TEM characterization. The authors thank Jun Xu and Jingmin Zhang in Electron Microscopy Laboratory, School of Physics, Peking University, for the help on the preparation of cross-sectional specimens and their TEM characterization. The author also thank to Beijing National Laboratory for Molecular Science. This work was financially supported by the Beijing Municipal Science & Technology Commission (No. Z181100004818001), the National Basic Research Program of China (No. 2016YFA0200101), and the National Natural Science Foundation of China (Nos. 21525310, 51432002, and 51520105003).

Conflict of Interest

The authors declare no conflict of interest.

Keywords

clean surface, contaminants, graphene, ultrahigh mobility

Received: May 9, 2019 Revised: August 15, 2019 Published online: September 10, 2019

- K. A. Reinhardt, R. F. Reidy, Handbook for Cleaning for Semiconductor Manufacturing: Fundamentals and Applications, John Wiley & Sons, USA 2011.
- [2] K. S. Novoselov, V. I. Fal'ko, L. Colombo, P. R. Gellert, M. G. Schwab, K. Kim, *Nature* **2012**, *490*, 192.
- [3] K. I. Bolotin, K. J. Sikes, Z. Jiang, M. Klima, G. Fudenberg, J. Hone, P. Kim, H. L. Stormer, Solid State Commun. 2008, 146, 351.
- [4] M. T. Pettes, I. Jo, Z. Yao, L. Shi, Nano Lett. 2011, 11, 1195.
- [5] Z. Li, Y. Wang, A. Kozbial, G. Shenoy, F. Zhou, R. McGinley, P. Ireland, B. Morganstein, A. Kunkel, S. P. Surwade, L. Li, H. Liu, Nat. Mater. 2013, 12, 925.
- [6] Z. Zhang, J. Du, D. Zhang, H. Sun, L. Yin, L. Ma, J. Chen, D. Ma, H. M. Cheng, W. Ren, Nat. Commun. 2017, 8, 14560.
- [7] Y. Kim, S. S. Cruz, K. Lee, B. O. Alawode, C. Choi, Y. Song, J. M. Johnson, C. Heidelberger, W. Kong, S. Choi, K. Qiao, I. Almansouri, E. A. Fitzgerald, J. Kong, A. M. Kolpak, J. Hwang, J. Kim, *Nature* 2017, 544, 340.

are governed by the applicable Creative Commons I

www.advancedsciencenews.com



www.advmat.de

- [8] S. Bae, H. Kim, Y. Lee, X. F. Xu, J. S. Park, Y. Zheng, J. Balakrishnan, T. Lei, H. R. Kim, Y. I. Song, Y. J. Kim, K. S. Kim, B. Ozyilmaz, J. H. Ahn, B. H. Hong, S. Iijima, *Nat. Nanotechnol.* 2010, 5, 574
- [9] Y. F. Hao, M. S. Bharathi, L. Wang, Y. Y. Liu, H. Chen, S. Nie, X. H. Wang, H. Chou, C. Tan, B. Fallahazad, H. Ramanarayan, C. W. Magnuson, E. Tutuc, B. I. Yakobson, K. F. McCarty, Y. W. Zhang, P. Kim, J. Hone, L. Colombo, R. S. Ruoff, *Science* 2013, 342, 720
- [10] Y. C. Lin, C. C. Lu, C. H. Yeh, C. Jin, K. Suenaga, P. W. Chiu, Nano Lett. 2012, 12, 414.
- [11] L.-W. Huang, C.-K. Chang, F.-C. Chien, K.-H. Chen, P. Chen, F.-R. Chen, C.-S. Chang, J. Vac. Sci. Technol., A 2014, 32, 050601.
- [12] J. Moser, A. Barreiro, A. Bachtold, Appl. Phys. Lett. 2007, 91, 163513.
- [13] N. Peltekis, S. Kumar, N. McEvoy, K. Lee, A. Weidlich, G. S. Duesberg, Carbon 2012, 50, 395.
- [14] G. Cunge, D. Ferrah, C. Petit-Etienne, A. Davydova, H. Okuno, D. Kalita, V. Bouchiat, O. Renault, J. Appl. Phys. 2015, 118, 123302
- [15] W. J. Choi, Y. J. Chung, S. Park, C. S. Yang, Y. K. Lee, K. S. An, Y. S. Lee, J. O. Lee, Adv. Mater. 2014, 26, 637.
- [16] A. M. Goossens, V. E. Calado, A. Barreiro, K. Watanabe, T. Taniguchi, L. M. K. Vandersypen, Appl. Phys. Lett. 2012, 100, 073110.
- [17] J. Robertson, Adv. Phys. 1986, 35, 317.
- [18] R. F. Zhang, Y. Y. Zhang, Q. Zhang, H. H. Xie, H. D. Wang, J. Q. Nie, Q. Wen, F. Wei, *Nat. Commun.* **2013**, *4*, 1727.
- [19] K. Kim, H. B. Lee, R. W. Johnson, J. T. Tanskanen, N. Liu, M. G. Kim, C. Pang, C. Ahn, S. F. Bent, Z. Bao, *Nat. Commun.* 2014, 5, 4781.
- [20] L. Lin, J. C. Zhang, H. S. Su, J. Li, L. Z. Sun, S. Lopatin, Y. H. Zhu, K. C. Jia, S. L. Chen, D. R. Rui, J. Y. Sun, R. W. Xue, P. Gao, N. Kang, Y. Han, H. Q. Xu, Z. Q. Tian, B. Ren, H. L. Peng, Z. F. Liu, Nat. Commun. 2019, 10, 1912.
- [21] L. Gao, G. X. Ni, Y. Liu, B. Liu, A. H. Castro Neto, K. P. Loh, *Nature* 2014, 505, 190.
- [22] X. Li, L. Colombo, R. S. Ruoff, Adv. Mater. 2016, 28, 6247.
- [23] F. Bonaccorso, Z. Sun, T. Hasan, A. C. Ferrari, *Nat. Photonics* 2010, 4, 611.

- [24] W. S. Leong, H. Wang, J. Yeo, F. J. Martin-Martinez, A. Zubair, P. C. Shen, Y. Mao, T. Palacios, M. J. Buehler, J. Y. Hong, J. Kong, Nat. Commun. 2019, 10, 867.
- [25] L. M. Malard, M. A. Pimenta, G. Dresselhaus, M. S. Dresselhaus, Phys. Rep. 2009, 473, 51.
- [26] F. Schwierz, Nat. Nanotechnol. 2010, 5, 487.
- [27] F. Xia, V. Perebeinos, Y. M. Lin, Y. Wu, P. Avouris, Nat. Nanotechnol. 2011. 6, 179.
- [28] S. V. Morozov, K. S. Novoselov, M. I. Katsnelson, F. Schedin, D. C. Elias, J. A. Jaszczak, A. K. Geim, Phys. Rev. Lett. 2008, 100, 016602.
- [29] J. H. Chen, C. Jang, S. Xiao, M. Ishigami, M. S. Fuhrer, Nat. Nanotechnol. 2008, 3, 206.
- [30] F. Pizzocchero, L. Gammelgaard, B. S. Jessen, J. M. Caridad, L. Wang, J. Hone, P. Boggild, T. J. Booth, *Nat. Commun.* 2016, 7, 11894
- [31] L. Banszerus, M. Schmitz, S. Engels, J. Dauber, M. Oellers, F. Haupt, K. Watanabe, T. Taniguchi, B. Beschoten, C. Stampfer, Sci. Adv. 2015. 1, e1500222.
- [32] R. R. Nair, P. Blake, A. N. Grigorenko, K. S. Novoselov, T. J. Booth, T. Stauber, N. M. R. Peres, A. K. Geim, *Science* 2008, 320, 1308.
- [33] R. C. Bansal, M. Goyal, Activated Carbon Adsorption, CRC Press, USA 2005.
- [34] H.-J. Butt, B. Cappella, M. Kappl, Surf. Sci. Rep. 2005, 59, 1.
- [35] S. P. Koenig, N. G. Boddeti, M. L. Dunn, J. S. Bunch, Nat. Nanotechnol. 2011. 6, 543.
- [36] B. Deng, Z. Pang, S. Chen, X. Li, C. Meng, J. Li, M. Liu, J. Wu, Y. Qi, W. Dang, H. Yang, Y. Zhang, J. Zhang, N. Kang, H. Xu, Q. Fu, X. Qiu, P. Gao, Y. Wei, Z. Liu, H. Peng, ACS Nano 2017, 11, 12337
- [37] X. Y. Zhang, Z. W. Xu, L. Hui, J. Xin, F. Ding, J. Phys. Chem. Lett. 2012, 3, 2822
- [38] J. Zhang, L. Lin, L. Sun, Y. Huang, A. L. Koh, W. Dang, J. Yin, M. Wang, C. Tan, T. Li, Z. Tan, Z. Liu, H. Peng, Adv. Mater. 2017, 29, 1700639.
- [39] S. W. Liu, H. P. Wang, Q. Xu, T. B. Ma, G. Yu, C. Zhang, D. Geng, Z. Yu, S. Zhang, W. Wang, Y. Z. Hu, H. Wang, J. Luo, *Nat. Commun.* 2017, 8, 14029.
- [40] H.-J. Buut, M. Jaschke, Nanotechnology 1995, 6, 1.